Thermal Denaturation of Spinach Plastocyanin: Effect of Copper Site Oxidation State and Molecular Oxygen†

Anders Sandberg,‡,§ David J. Harrison,||,§ and B. Göran Karlsson*,||,⊥

Department of Chemistry and Bioscience, Chalmers University of Technology, Box 462, 405 30 Göteborg, Sweden, and Department of Chemistry, University of Göteborg, Box 462, 405 30 Göteborg, Sweden

Received March 7, 2003; Revised Manuscript Received June 12, 2003

ABSTRACT: The thermal denaturation of the cupredoxin plastocyanin (PC) from spinach has been studied with the aim of improving the understanding of factors involved in the conformational stability of antiparallel β-sheet proteins. Studies using differential scanning calorimetry have been complemented with nuclear magnetic resonance spectroscopy, absorbance spectroscopy, dynamic light scattering, and mass spectrometry in elucidation of the effect of the copper-site oxidation state on the irreversible thermal denaturation process. Our results indicate that copper-catalyzed oxidation of the metal-ligating cysteine is the sole factor resulting in thermal irreversibility. However, this can be prevented in reduced protein by the removal of molecular oxygen. Application of a two-state equilibrium transition model to the folding process thus allowed the extraction of thermodynamic parameters for the reduced protein ($\Delta_{trs}H$ = 494 kJ mol^{-1}, ΔH_{vH} = 343 kJ mol^{-1}, and T_m = 71 °C). However, anaerobically denatured oxidized protein and all aerobically denatured species undergo covalent modification as a result of the copper-catalyzed oxidation of the metal-ligating cysteine residue resulting in the formation of both oxidized monomers and disulfide-linked dimers. On the basis of these results, a general mechanism for the irreversible thermal denaturation of cupredoxins is proposed. The results presented here also indicate that PC, as opposed to the previously characterized homologous protein azurin, unfolds via at least one significantly populated intermediate state ($\Delta H_{vH}/\Delta_{trs}H$ = 0.7) despite the almost identical native state topologies of these proteins. These findings will aid the characterization of the stability of PC and other cupredoxins and possibly of all cysteine-ligating metal-binding proteins.

Plastocyanin (PC)[1] from spinach is a small (10.4 kDa) eight-stranded β-sheet protein of Greek-key topology that belongs to the cupredoxin family. The physiological role of this copper-binding protein is to function as a mobile electron carrier between the cytochrome b_6f complex and photosystem I during photosynthesis (*1*−*3*). The first structure of PC, that from poplar, was determined in 1978 (*4*), but wild-type plastocyanin from spinach has consistently failed to crystallize. However, the mutant Gly8Arg readily does, and its oxidized (Cu^{2+}) structure was eluded by X-ray crystallography to a resolution of 1.3 Å (Figure 1) (*5*). Comparing the crystal structure with the nuclear magnetic resonance (NMR) solution structure of the reduced (Cu^{+}) wild-type protein (*6*), only minor structural differences are detected as a result of the mutation and the different redox states. This latter finding is corroborated by the finding that there are no significant differences in the dynamic properties or the solution structures of reduced and oxidized plastocyanin from *Synechocystis* sp. PCC6803 (*7*). A constrained metalloprotein active site has functional significance in that the protein fold modulates the physical properties of the copper ion so that its reduction potential and the reorganization energy of electron transfer are finely tuned to match the protein's redox partners (*8*). In particular, the native form of spinach PC coordinates the copper ion in a type 1 center with four fixed ligands—three equatorial (Cys84, His37, and His87) and one axial (Met92). This type of 4[$N_2S(S)$] trigonal pyramidal coordination of the copper ion confers a reduction potential of 380 mV (vs NHE) on PC.

The surface of PC is characterized by two prominent acidic patches conserved in plants and one hydrophobic patch conserved among all different biological species (*1*, *3*). These patches are believed to be involved in the molecular recognition, orientation, and interaction between PC and its redox partners. Novel NMR methodologies involving mapping of chemical shift perturbations (*9*, *10*) and intermolecular pseudocontact shifts (*11*), combined with rapid spectroscopic techniques (e.g., refs *12*−*14*) have been crucial in probing the contribution of hydrophobic and electrostatic interactions during complex formation. In conjunction with theses techniques, the use of specific PC mutants has helped

† This work was supported by a grant from the Research Training Network "TRANSIENT" in the Human Potential Program of the European Commission HPRN-CT-1999-00095 and also from the Carl Trygger Foundation.

* To whom correspondence should be addressed. Telephone: +46 317733881. Fax: +46 317733880. E-mail: Goran.Karlsson@molbiotech.chalmers.se.

‡ University of Göteborg.

§ These authors contributed equally to this work.

|| Chalmers University of Technology.

⊥ Current address: Swedish NMR Centre, University of Göteborg, Box 465, 405 30 Göteborg, Sweden.

[1] Abbreviations: PC, plastocyanin; DSC, differential scanning calorimetry; NMR, nuclear magnetic resonance; DLS, dynamic light scattering; ESI MS, electrospray ionization mass spectrometry; T_m, transition temperature; $\Delta_{trs}H$, transition enthalpy; ΔH_{vH}, van't Hoff enthalpy; EPR, electron paramagnetic resonance; DSS, 2,2-dimethyl-2-silapentane-5-sulfonic acid; C_p, excess heat capacity; UV, ultraviolet.

10.1021/bi034371e CCC: $25.00
Published on Web 08/06/2003

FIGURE 1: 3-D crystal structure of the Gly8Asp mutant of spinach plastocyanin (*5*) showing the cupric ion and the main equatorial ligands (His37, His87, and Cys84) as well as the minor axial ligand (Met92). The picture was drawn using Swiss PDB viewer (*47*).

to elucidate the influence of individual residues during transient complex formation and electron transfer (*12*−*14*).

When PC mutants are to be used in interaction studies, it is important to confirm that they retain their structural integrity, especially during prolonged NMR experiments in a detergent-rich environment. Prediction of the effect of a mutation on the conformational stability of a given protein is, however, difficult because of the inherent complexity of protein folding. Thus, detailed comparisons of mutations in a protein are best achieved experimentally, where temperature-induced denaturation is considered to give more complete thermodynamic information than chemically induced denaturation studies (*15*). For thermal analysis of protein stability, differential scanning calorimetry (DSC) is increasingly used for quantitative measurements of the heat changes accompanying the thermal melting of polypeptide chains (*16*). Ideally, the protein should be able undergo complete and reversible cooperative thermal unfolding, thus allowing thermodynamic equilibrium transition models to be applied directly to the calorimetric data, and a transition temperature (T_m), a transition enthalpy ($\Delta_{trs}H$), and a van't Hoff enthalpy (ΔH_{vH}) to be extracted accordingly (*17*). However, many proteins are unable to reversibly thermally unfold, a situation commonly attributed to intermolecular aggregation and degradative covalent reactions occurring at high temperatures (*18*−*20*).

An earlier investigation of spinach PC thermal stability indicated that under aerobic conditions the reduced protein was more thermostable (T_m = 71 °C) than the oxidized form (T_m = 61 °C) (*21*). On cooling, the end state of neither protein resembled the wild-type protein, and in the case of the reduced PC resulted in two distinct final states. Reduced PC under anaerobic conditions was observed to have a T_m greater than 100 °C. The irreversibility of thermal unfolding of oxidized spinach PC was later confirmed by DSC, absorbance spectroscopy, and electron paramagnetic resonance (EPR) spectroscopy (*22*). Intermolecular aggregation and degradative covalent modifications at temperatures greater than T_m were suggested to account for this irreversibility, thus following the general Lumry−Eyring scheme

$$N \leftrightarrows U \rightarrow D \qquad (1)$$

where N is the native protein, U is the reversibly unfolded protein, and D is the irreversibly denatured protein. It is generally assumed that the slow kinetic nature of the irreversible step, as observed by its dependence on the heating scan rate, allows separation of the irreversible and reversible steps (*23*, *24*). Thus, by determining the dependence of the heat capacity changes of PC on the scan rate, these changes were extrapolated to infinite scan rate, and thermodynamic parameters for the reversible step alone were extracted (T_m = 69 °C, $\Delta_{trs}H$ = 254 kJ mol^{-1}) (*22*).

The closely related cupredoxin azurin has recently been the subject of similar studies (*25*). It was concluded that copper-catalyzed oxidation of the metal-coordinating cysteine sulfur was the primary cause of thermal irreversibility. Irreversibility was thereby prevented by removal of dissolved O_2, and equilibrium transition models could thus be applied to the calorimetric data for azurin coordinating nonreducible metal cofactors (i.e., Cu^+ and Zn^{2+}) under anaerobic conditions.

In the present study, we have investigated the thermal denaturation of both oxidized and reduced spinach PC under both aerobic and anaerobic conditions. We demonstrate that reduced PC, when under anaerobic conditions, undergoes reversible thermal unfolding thus allowing direct extraction of thermodynamic parameters. Under the other three conditions, DSC is used to observe the complex thermodynamics occurring during the irreversible thermal denaturation of PC. A possible mechanism to explain this irreversible unfolding is proposed with the aid of further data from NMR, electrospray ionization mass spectrometry (ESI MS), dynamic light scattering (DLS), and absorbance spectroscopy. The formation of refoldable PC disulfide dimers during thermal unfolding has also been confirmed. Furthermore, monitoring the reversible unfolding of reduced PC using NMR reveals a significant difference in T_m as observed with other techniques. These findings will aid further characterization of the stability of plastocyanin and other cupredoxins, as well as increase our understanding of how nature performs complex redox chemistry.

EXPERIMENTAL PROCEDURES

Materials. All stock chemicals were reagent grade from Merck except where stated. Deionized water was used in all measurements.

Protein Expression and Purification. Wild-type spinach PC was expressed in *Escherichia coli* RV308 and purified as previously described (*26*). The final anion-exchange step using a Resource-Q column (Pharmacia) was repeated until the oxidized PC had an $A_{277\ nm}/A_{597\ nm}$ ratio ≤1.1. Aliquots were frozen in liquid nitrogen and stored at −24 °C until use. An extinction coefficient of 4700 M^{-1} cm^{-1} at both 277 and 597 nm was used for oxidized protein (*26*), and this

extinction coefficient was adjusted to 7500 M^{-1} cm^{-1} for the $A_{277\ nm}$ of reduced PC (*27*). However, amino acid analysis (by the Amino acid Analysis Center, Department of Biochemistry, Uppsala University) was carried out to more accurately determine the concentration of PC in the calorimetric experiments since the $\Delta_{trs}H$ is dependent on protein concentration whereas ΔH_{vH} is not.

Sample Preparation. For experiments with oxidized PC, samples were fully oxidized by addition of potassium ferricyanide (Sigma). Oxidant was then removed from the protein by passage twice through a PD10 Sephadex G-25 M gel filtration column (Pharmacia). Likewise, for experiments with reduced PC, samples were reduced using ascorbic acid (Sigma), with reductant being removed as above. Oxidation state and copper occupancy were determined by measurement of the $A_{277\ nm}/A_{597\ nm}$ ratio, which ideally should be equal to unity (*26*). Samples for use under anaerobic conditions were deoxygenated by being placed in airtight vials, and N_2 gas was bubbled through the samples for at least 30 min prior to use.

DSC Measurements and Analysis. DSC measurements were performed using a VP-DSC Microcalorimeter (Microcal, Inc.) consisting of a matched pair of 0.511 mL cells. All scans were preequilibrated at 15 °C for 15 min and then scanned twice from 15 to 100 °C (anaerobic samples) or 120 °C (aerobic samples) at a scan rate of 60 °C h^{-1}. In addition, a second anaerobic experiment on reduced PC was performed to assess the extent of reversibility, and hence, was only scanned to 90 °C where the transition profile returned to the post-transitional baseline. Data were collected every 10 s for all samples except the deoxygenated reduced samples, for which data were collected every 16 s. The second of two buffer versus buffer scans was used as a baseline and subtracted from the calorimetric profiles. Sample solutions were 0.08 mM, and buffer was 10 mM potassium phosphate pH 7.0. For the scans run under oxygen-free conditions, the sample cell was purged with N_2 gas prior to injection of the sample. Deoxygenated samples were kept in airtight containers and transferred to the calorimeter through the septum using gastight syringes and a steady flow of N_2 gas to minimize the risk of O_2 contamination.

All DSC scans were analyzed using the EXAM software program (*28*). EXAM determines the pre- and post-transitional baselines from least-squares fits of straight lines to the data points and calculates a sigmoidal baseline from the extent of the reaction by employing the profile of the transition peak. A two-state A $\leftrightarrows$ B transition model was used to obtain the T_m and $\Delta_{trs}H$ of the transition. For the irreversible transitions, redox reactions in the denatured state severely obscure the profiles at $T > T_m$. However, considering that the irreversible processes occur exclusively in the denatured state and are fairly slow, they can be assumed to be negligible at $T < T_m$, and so a theoretical transition was calculated for the profile at $T > T_m$ for illustrative purposes and to obtain a more accurate T_m than by visual inspection alone. The sigmoidal baselines calculated by EXAM were used as estimates of the true baselines. These were fitted in the Igor Pro program (Wavemetrics) to determine the ΔH_{vH} as described previously (*29*, *30*). Uncertainties reported are a combination of errors from the curve fitting procedure and imprecision in temperature readings (±0.1 °C).

Absorbance Spectroscopy. Thermal denaturation of PC was monitored using a Cary 4 UV/visible spectrophotometer calibrated with a digital thermometer inserted into the cuvette. A scan rate of 60 °C h^{-1} was used between 25 and 90 °C, and $A_{277\ nm} - A_{262\ nm}$ and $A_{597\ nm}$ were plotted against temperature. Scan-rate dependence of the reversible transition was analyzed by a repeat experiment at a scan rate of 30 °C h^{-1}. Data were analyzed as above using the Igor Pro program. Concentrations were 0.1 mM PC in 10 mM potassium phosphate buffer pH 7.0. Errors reported are a combination of those of the curve fitting and of the temperature readings (±0.5 °C).

NMR Measurements. Reduced PC used for the NMR measurements was at 1 mM in 10 mM phosphate buffer, pH 7.0, 10% D_2O, and 1 mM 2,2-dimethyl-2-silapentane-5-sulfonic acid (DSS) as reference. The sample was deoxygenated and sealed in a restricted NMR tube. 1-D spectra were recorded with 64 transients, 32 000 points, and a sweep width of 20 kHz on an 800 MHz Varian spectrometer. Spectra were recorded as the protein was heated from 30 to 80 °C and back down to 30 °C, with 2 °C increments during the unfolding transition and a 5 min equilibration period after each temperature change. Temperature calibration was performed under identical conditions using 100% ethylene glycol (*31*). NMR data were then processed using MestRe-C 2.3a program (http://qobrue.usc.es). The chemical shifts of the reduced spinach PC have been assigned previously (*6*, *32*). The combined peak area of the resonances of the methyl-group protons Val96 H^{γ} and Leu12 H^{δ}, as well as both peaks of Leu74 H^{δ} and Val39 H^{γ} (cf. Figure 3), were plotted as a function of temperature, and the data were analyzed in Igor Pro as described above for the extraction of T_m and ΔH_{vH}. Errors reported are of the curve fitting procedure.

Dimer Preparation and Analysis. An anaerobic sample of 0.1 mM oxidized PC, in 10 mM potassium phosphate buffer pH 7.0, was heated from 25 to 85 °C at a 60 °C h^{-1} scan rate and then cooled back down to 25 °C at a rate of 30 °C h^{-1}. An aliquot of the sample was analyzed by size-exclusion chromatography using a Superdex 200 HR 10/300 column (Pharmacia) in line with a mini-DAWN Light Scattering system (Wyatt Technology Corp.) at a laser wavelength of 690 nm. The flow-rate was 0.3 mL min^{-1}. The Mini-DAWN LS system was operated with the Astra software (Wyatt Technology Corp.), and data were analyzed according to the manufacturer's instructions.

A second aliquot of the sample was subjected to ESI MS on a Q-Tof mass spectrometer (Micromass) equipped with a nanospray ion source. The sample was dissolved in pure water supplemented with 0.1% formic acid, and the nanospray needle voltage was +900 V. Mass spectral data were analyzed with the MassLynx3.4 software.

RESULTS

Reduced PC, Anaerobic. A typical calorimetric profile of the thermal denaturation of reduced PC under anaerobic conditions is presented in Figure 2A (parameters in Table 1). This transition was fitted to a two-state transition model (*28*) giving a T_m of 71.2 ± 0.1 °C. The subsequent rescan produced a transition with a nearly identical T_m (71.9 ± 0.1 °C) thus confirming the reversibility of the unfolding process. Reversibility of the thermal unfolding allowed extraction of

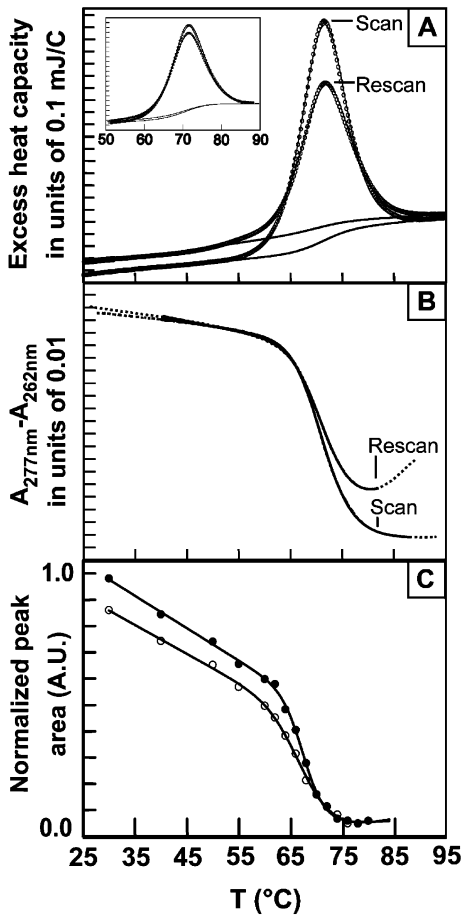

FIGURE 2: Anaerobic thermal denaturation of reduced spinach plastocyanin. (A) DSC scan and rescan at 60 °C h^{-1}. Sample was scanned twice from 15 to 100 °C (open circles), and the transitions were fitted to a two-state model with calculated baseline (solid line). The inset shows an additional experiment with scan and rescan at 60 °C h^{-1} from 15 to 90 °C with similarly fitted functions. Sample volumes were 0.511 mL, and concentrations of plastocyanin were 0.08 mM in 10 mM potassium phosphate pH 7.0. (B) Temperature scanning absorbance measurements of 0.1 mM plastocyanin at 60 °C h^{-1} between 25 and 90 °C (broken lines) with least-squares fitted functions (solid lines). Concentration of the protein was 0.10 mM in 10 mM potassium phosphate pH 7.0. (C) Analysis of the combined methyl peak area (cf. Figure 3) as determined by 1-D ^{1}H NMR showing unfolding (filled circles) and refolding transitions (empty circles) with least-squares fitted functions (solid lines). Concentration of plastocyanin was 1.0 mM in 10 mM potassium phosphate pH 7.0, 1 mM DSS, and 10% D_2O.

ΔH_{vH} (343 ± 0.5 kJ mol^{-1}) and $\Delta_{trs}H$ (494 ± 27 kJ mol^{-1}) for the first scan. However, the $\Delta H_{vH}/\Delta_{trs}H$ ratio of 0.7 indicates that the unfolding may proceed via intermediate states (*16*, *17*). A colorless solution with no precipitate was observed upon visual examination of the sample after the rescan.

To test the extent of reversibility, a repeat experiment was conducted with the heating during the first scan stopped when the peak of the endothermic transition returned to the baseline at 90 °C. The subsequent scan resulted in a second transition with the two peaks differing in area by only 7% (Figure 2A, inset), suggesting reversibility of greater than 90%. Furthermore, both scans had identical T_ms (71.0 ± 0.1 °C). Again, no precipitate was observed by visual inspection of the sample after the rescan.

The unfolding transition was subsequently investigated by absorbance spectroscopy (Figure 2B; parameters in Table 1), resulting in a single transition with a T_m of 71.0 ± 0.5 °C and a ΔH_{vH} of 342 ± 3 kJ mol^{-1}. Reversibility was confirmed by the single transition observed in the rescan, having a T_m of 71.5 ± 0.5 °C and a ΔH_{vH} of 335 ± 2 kJ mol^{-1}. Scan-rate dependence was deemed negligible from the repeat experiment at a scan rate of 30 °C h^{-1}, which resulted in a two-state sigmoidal transition with a T_m of 70.7 ± 0.5 °C and a ΔH_{vH} of 326 ± 2 kJ mol^{-1} (data not shown).

NMR was used to further investigate the thermal unfolding of PC at elevated temperatures. 1-D ^{1}H spectra were recorded within the temperature range of 30−80 °C. Comparison of the 1-D spectra recorded before and after heating confirms that the protein retains its native structure upon refolding (Figure 3A). It was noted that the chemical shift of the copper ligating residues His37 $H^{\epsilon 2}$ (11.64 ppm) and His87 $H^{\epsilon 1}$ (7.74 ppm) returned to their original shift on refolding (not shown), thus confirming that the type 1 copper site is reformed with bound metal. The six methyl-group protons Val96 H^{γ}, Leu12 H^{δ}, Val39 $H^{\gamma 1}$, Val39 $H^{\gamma 2}$, Leu74 $H^{\delta 1}$, and Leu74 $H^{\delta 2}$ were well-resolved throughout the unfolding transition (Figure 3B). Analysis of their combined peak area at each temperature resulted in a single transition (Figure 2C; parameters in Table 1). The unfolding of this transition had a T_m of 67.9 ± 0.4 °C and ΔH_{vH} of 483 ± 56 kJ mol^{-1}, and the refolding transition had a similar T_m of 67.8 ± 0.7 °C and ΔH_{vH} of 317 ± 39 kJ mol^{-1}. Identical transitions were seen if the different peaks were analyzed separately, indicating global unfolding, as the four residues are evenly spread over the entire structure. The absence of aggregates after refolding, as determined by visual examination, was deemed as significant because of the high concentration of protein in this sample (1 mM).

Reduced PC, Aerobic. The first DSC scan of reduced PC in the presence of molecular oxygen (Figure 4A; parameters in Table 1) revealed a large positive endotherm interrupted by a complex negative exothermic phase, possibly consisting of three separate exothermic peaks. On rescanning the sample, two small endothermic transitions were seen that by visual inspection had T_ms of 53 and 79 °C, respectively, yet as no peak was observed that coincided with that of the endothermic peak seen on the first scan, the unfolding process was regarded as being irreversible. A colorless sample with no precipitation was observed on visual inspection after the rescan.

Since no scan-rate dependence was undertaken in this study, an attempt was instead made to fit a two-state transition model to the initial section of the endothermic phase of the first scan (Figure 4B; parameters in Table 1). The irreversible reactions occur mainly at $T \geq T_m$ and are fairly slow, extending over a time period exceeding 20 min. Therefore, data points extending roughly from the T_m to the return of the exotherm to the baseline (at approximately 98 °C) were neglected during the curve-fitting procedure. This allowed estimation of $T_m = 71.0 \pm 0.1$ °C, equal to that of the reduced PC under anaerobic conditions. Calculation of the ΔH_{vH} from the baseline estimated by EXAM gave a value similar to that of the reversible reaction (358 ± 0.5 kJ mol^{-1}). However, the transition enthalpy could not be determined reliably because of the irreversible redox chemistry occurring during the transition. Comparing the change in specific excess heat capacity (C_p) between the two reduced PC samples in going from 50 °C (fully folded) to 100 °C (fully

Table 1: Thermodynamic Parameters of the Thermal Unfolding of PC

	$A_{597\ nm}$		$A_{277\ nm} - A_{262\ nm}$		DSC			NMR	
	T_m (°C)	ΔH_{vH} (kJ mol^{-1})	T_m (°C)	ΔH_{vH} (kJ mol^{-1})	T_m (°C)	ΔH_{vH} (kJ mol^{-1})	$\Delta_{trs}H$ (kJ mol^{-1})	T_m (°C)	ΔH_{vH} (kJ mol^{-1})
reduced, aerobic					71.0 ± 0.1 (53[a], 79[a])[b]	358 ± 0.5			
reduced, anaerobic			71.0 ± 0.5 (71.5 ± 0.5)	342 ± 3 (335 ± 2)	71.2 ± 0.1 (71.0 ± 0.1)	343 ± 0.5	494 ± 27	67.9 ± 0.4 (67.8 ± 0.7)	483 ± 56 (317 ± 39)
oxidized, aerobic	63.5 ± 0.5	468 ± 6			67.8 ± 0.1 (53[a], 79[a])	354 ± 0.3			
oxidized, anaerobic	63.8 ± 0.5	467 ± 5			67.2 ± 0.1, 75.0 ± 0.2 (53[a], 78.7 ± 0.1)	352 ± 0.7, 648 ± 2 (432 ± 0.4)			

[a] Values obtained from visual inspection only. [b] Values in parentheses indicate parameters extracted on rescan.

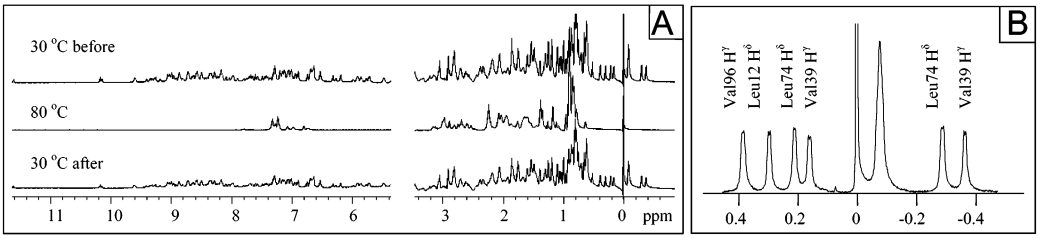

FIGURE 3: 1-D NMR spectroscopic thermal analysis of 1.0 mM reduced spinach plastocyanin under anaerobic conditions. (A) Spectra recorded before (30 °C), during (80 °C), and after (30 °C) thermal denaturation. (B) Methyl region displaying the six methyl peaks monitored during unfolding and refolding. The sample contained 10% D_2O, 1 mM DSS, and 10 mM potassium phosphate pH 7.0.

unfolded/denatured), the change is somewhat larger for the anaerobic reversible transition (+0.917 kJ K^{-1} g^{-1}) than for the aerobic irreversible transition (+0.870 kJ K^{-1} g^{-1}), reflecting different end states.

Absorbance spectroscopy of the unfolding transition was similarly complex with at least two transitions observed (Figure 4C). The first transition is followed by a second smaller transition, during which the signal actually increases before finally decreasing again. Difficulties in predicting the post transitional baselines hindered the fitting of any of the transitions, thus preventing extractions of T_m. No transition was observed upon a rescan.

Oxidized PC, Aerobic. During the first DSC scan, a large endothermic peak was again seen, yet the two-state transition-like symmetry was interrupted by a complex exothermic phase. This exotherm could consist of two separate exothermic peaks or of a single exotherm interrupted by a small endotherm around 80−85 °C (Figure 5A). Our present data do not allow us to distinguish between these alternatives. Upon a rescan, two small endothermic peaks are again seen that by visual inspection had a T_m of 53 and 79 °C, respectively (see Table 1), yet as no peak is observed that coincides with that of the endothermic peak seen on the first scan, the unfolding process is again regarded as being irreversible. After the rescan, the sample was colorless and without precipitation.

As with the reduced aerobic sample above, attempts were made to fit a two-state transition model to the initial section of the endothermic phase of the first scan (Figure 5B; parameters in Table 1). This allowed estimation of T_m = 67.8 ± 0.1 °C, thus confirming that oxidized PC is less thermostable than reduced PC (*21*). Furthermore, calculation of the ΔH_{vH} as above gave a value of 354 ± 0.3 kJ mol^{-1}, which is nearly identical to the value for the reduced aerobic sample. No transition enthalpy was calculated because of the complex irreversible redox chemistry that occurs during the transition and that inevitably leads to different end states.

Absorbance spectroscopy measured at 597 nm, which monitors the environment of the copper center, displayed a single irreversible transition for the first scan that was fitted to a two-state transition model with T_m = 63.5 ± 0.5 °C (data not shown; parameters in Table 1). The ΔH_{vH} for this transition was 468 ± 6 kJ mol^{-1}. However, monitoring absorbance in the far UV region, two transitions are clearly visible during the first scan (Figure 5C). Difficulties in predicting the post-transitional baselines hindered the fitting of any of the transitions, thus preventing extractions of T_m. No transitions at either wavelength were observed during subsequent rescans.

Oxidized PC, Anaerobic. During the first DSC scan, a large endotherm was interrupted by a second, smaller endothermic peak, which itself ended in a minor exothermic phase (Figure 6A). On rescan, two endothermic peaks were again observed, but while the first peak was small, the second peak was substantially larger. A colorless solution with no precipitation was again observed after the rescan.

The two peaks of the first scan were analyzed separately (Figure 6B; parameters in Table 1) and fitted to a two-state transition model giving a T_m of 67.2 ± 0.1 °C and a ΔH_{vH} of 352 ± 0.7 kJ mol^{-1} for the first transition and a T_m of 75.0 ± 0.2 °C and a ΔH_{vH} of 648 ± 2 kJ mol^{-1} for the second. The inset in Figure 6B shows the larger endothermic peak observed on the second scan also fitted to a two-state transition model with a T_m of 78.7 ± 0.1 °C and a ΔH_{vH} of 432 ± 0.4 kJ mol^{-1} (Table 1). No $\Delta_{trs}H$ was calculated for these transitions.

Absorbance spectroscopy measured at 597 nm displayed a single transition for the first scan that was fitted to a two-state transition model with a T_m = 63.8 ± 0.5 °C and a ΔH_{vH} of 467 ± 5 kJ mol^{-1}, yet no transition was observed during

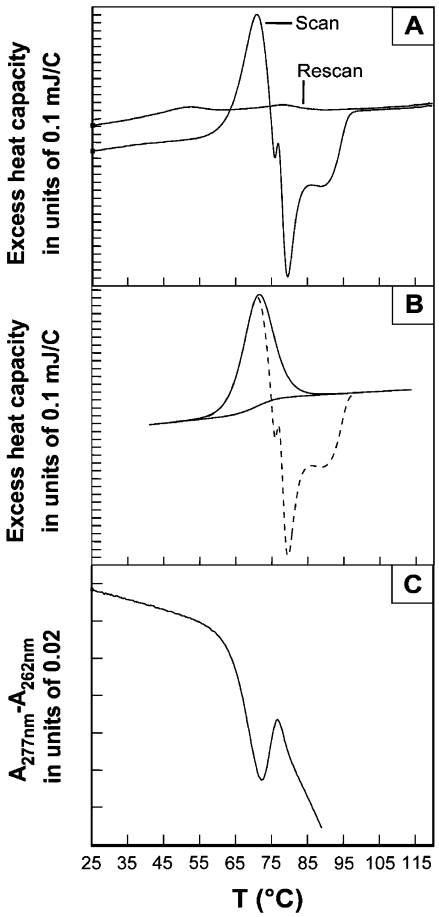

FIGURE 4: Aerobic thermal denaturation of reduced spinach plastocyanin. (A) DSC scan and rescan from 25 to 120 °C at 60 °C h^{-1}. Sample volume was 0.511 mL, and protein concentration was 0.08 mM in 10 mM potassium phosphate pH 7.0. (B) Least-squares fit of a two-state transition model (solid line) to the major positive endotherm of the DSC scan, using data points up to approximately the T_m. Also displayed are the fitted baseline (solid line) and the thermogram (broken line). (C) Temperature scanning absorbance measurements at 60 °C h^{-1} between 25 and 90 °C. Protein concentration was 0.10 mM in 10 mM potassium phosphate buffer pH 7.0.

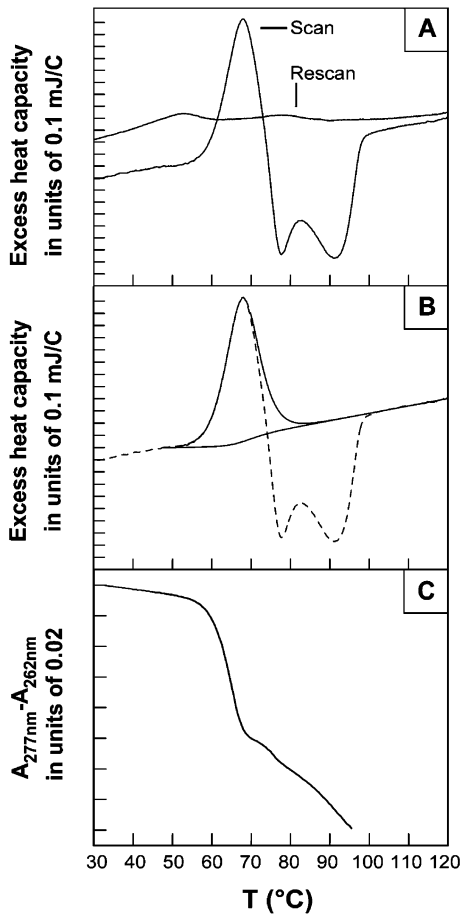

FIGURE 5: Aerobic thermal denaturation of oxidized spinach plastocyanin. (A) DSC scan and rescan. This sample was scanned from 15 to 120 °C at a scan rate of 60 °C h^{-1}. Sample volume was 0.511 mL and concentration of protein was 0.08 mM in 10 mM potassium phosphate buffer pH 7.0. (B) Least-squares fit of a two-state transition model (solid line) to the major endothermic peak of the DSC scan, using data points up to approximately the T_m. Also displayed are the calculated baseline (solid line) and the thermogram (broken line). (C) Temperature scanning absorbance measurements at 60 °C h^{-1}. Protein concentration was 0.10 mM in 10 mM potassium phosphate pH 7.0.

the second scan (data not shown; parameters in Table 1). Absorbance spectroscopy in the far UV region during the first scan (Figure 6C) indicated a large transition followed by a smaller one, both of which roughly coincide with the transitions seen in the DCS data. Because of the multiphasic nature of the transition, and the difficulties in predicting the post-transitional baseline, the fitting of these data was deemed as too unreliable and therefore not undertaken. Upon a rescan, a minor transition was detected with a T_m of 77 °C (data not shown).

To further investigate the transition observed during a rescan, a sample of oxidized PC under anaerobic conditions was heated to 85 °C (the temperature at the end of the endothermic phase detected during the first DSC scan) and then cooled back to 25 °C. The sample was then subjected to size-exclusion chromatography-linked dynamic light-scattering analysis (Figure 7). Two separate peaks were clearly observed in the chromatogram, with the light-scattering analysis indicating that they contained molecules of sizes of approximately 20 and 10 kDa, respectively (not shown). The sample was also analyzed by ESI MS, with several species detected: 10413, 10449, 20824, 20923, and 21023 Da of which the last two were minor (data not shown) with the expected masses for nonoxidized monomer and dimer being 10413 and 20826 Da, respectively.

DISCUSSION

In this study, we demonstrate that upon removal of dissolved molecular oxygen from the solution, reduced spinach plastocyanin exhibits reversible thermal unfolding in analogy with previous findings for the homologous protein *Pseudomonas aeruginosa* azurin (*25*). Although both of these proteins display the cupredoxin fold (an eight-stranded β-sheet protein of Greek-key topology) and have similar arrangements of the main metal binding ligands, they share only ca. 20% sequence identity. This rather low similarity is reflected in a number of differences, including the lack of an α-helix in plastocyanin, as well as plastocyanin having a longer loop that surrounds the copper site. In addition, the copper site is much more buried in azurin than it is in plastocyanin. As one of the main causes of thermal irreversibility in monomeric proteins appears to be the degradative reactions occurring at high temperatures (*18*, *19*), it is thus

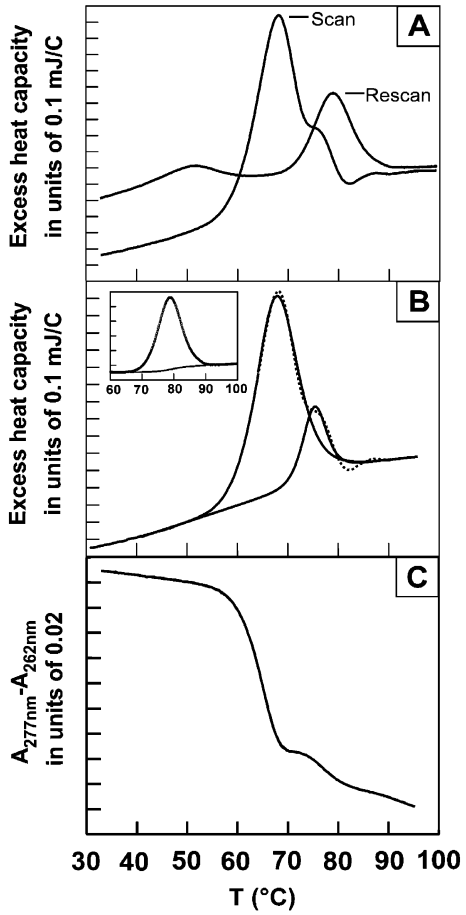

FIGURE 6: Anaerobic thermal denaturation of oxidized spinach plastocyanin. (A) DSC scan and rescan from 15 to 100 °C at 60 °C h^{-1}. Concentration of protein was 0.08 mM in 10 mM potassium phosphate pH 7.0. Sample volume was 0.511 mL. (B) Peak separation of the endotherm of the first scan (broken line) with the resulting least-squares fit of the two curves to a two-state transition model (solid lines). Inset shows the fit to a two-state transition model of the second exothermic peak on the rescan and fitted baseline. (C) Temperature scanning absorbance measurements at 60 °C h^{-1} between 25 and 90 °C. Plastocyanin concentration was 0.10 mM in 10 mM potassium phosphate pH 7.0.

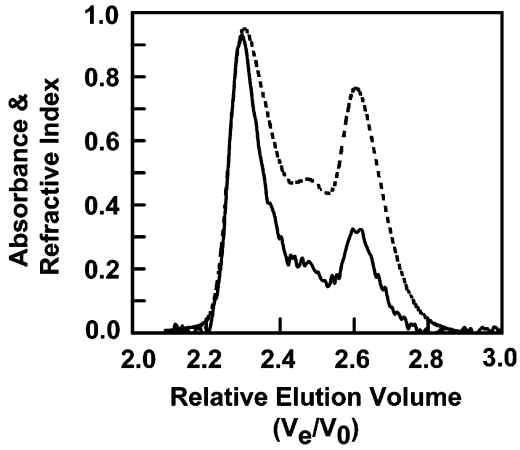

FIGURE 7: Size-exclusion chromatography and dynamic light scattering of a heat-treated sample of oxidized spinach plastocyanin under anaerobic conditions. A 0.10 mM plastocyanin sample in 10 mM potassium phosphate pH 7.0 was heated to 85 °C, slowly cooled back to 25 °C, and then applied to a size-exclusion column at a rate of 0.3 mL min^{-1}. The relative elution volume is defined as V_e (the elution volume) over V_0 (the void volume). Absorbance was collected at 280 nm (broken line), and the refractive index was collected at a laser wavelength of 690 nm (solid line).

expected to be dependent on sequence specific factors. However, because of the fairly low sequence similarity between PC and azurin, their similar behavior suggests that thermal reversibility in the cupredoxins is mainly controlled by native state topological factors, as these are the major determinants of the folding free-energy landscape (*33*). This is in agreement with the previous finding for two bacterial α-amylases, where both aggregate as a result of the formation of incorrect (misfolded) structures rather than covalent modifications of the proteins (*20*).

DSC data for the reversible thermal denaturation of reduced PC (Figure 2A) were treated with a two-state equilibrium transition model (*28*), resulting in a transition enthalpy of 494 kJ mol^{-1} (Table 1), which corresponds to a specific transitional enthalpy of 47.4 J g^{-1}. This is slightly higher than that found for reduced wild-type azurin—the average of the $\Delta_{trs}H$ at 40 and 80 °C h^{-1} scan rates is 35.4 J g^{-1} (496 kJ mol^{-1}) for this azurin derivative (*25*). This indicates a larger relative exposed hydrophobic surface area in unfolded PC and, since reduced azurin melts 14 °C higher than reduced PC, reflects that the additional stabilization of azurin is due to a disulfide bond that is lacking in PC. This type of destabilization of the unfolded state ensemble is commonly believed to be mainly of entropic origin (*34*, *35*).

While the thermal denaturation for the reduced anaerobic PC sample as observed by NMR, absorbance spectroscopy, and DSC exhibited reversible single transitions that were readily fitted to a two-state thermodynamic model (see Figure 2), the $\Delta H_{vH}/\Delta_{trs}H$ ratio of 0.7 as calculated from DSC data suggests that unfolding involves at least one significantly populated intermediate state (*16*, *17*). This is an unexpected finding, as no such intermediates were identified in azurin (*25*), and proteins of nearly identical topology are expected to have very similar folding landscapes (*33*). However, native spinach PC has two out of its five prolines in cis configuration, and a long-lived kinetic refolding intermediate trapped by the presence of an incorrect proline isomer has previously been identified in French bean apo-PC (*36*). The $\Delta H_{vH}/\Delta_{trs}H$ ratio might therefore reflect a broadening of the DSC profile caused by this trapped intermediate.

To be able to more qualitatively follow the thermal unfolding and refolding process of reduced PC under anaerobic conditions, a series of 1-D NMR spectra was recorded as a function of temperature. No obvious intermediate was detected, but analysis of the NMR peak area during thermal unfolding and refolding (Figure 2C) reports a transition with a T_m that is 3 °C below that as determined by DSC and absorbance spectroscopy (see Table 1). The NMR experiment probes the environment of six upshifted methyl group protons from four residues spread out over the entire structure, and their chemical shifts are sensitive even to minute structural perturbations. Meanwhile, DSC monitors the solvation of hydrophobic residues and should therefore reflect unfolding of the whole protein. The data reported here are consistent with a pre-transitional alteration of the native state, which has been demonstrated previously (*37*, *38*). It appears as if a loosening of the compact native state of proteins may occur before the onset of denaturation (*37*, *38*). We believe that the decrease in spatial constraints from such a loosening of the compact protein structure may be detected by NMR but not by DSC or UV absorbance spectroscopy.

That the differences in T_m are due to a concentration-dependent reversible aggregation effect that perturbs the equilibrium is unlikely, as such an effect is expected to exhibit scan-rate dependence (*39*), which was not observed.

A pre-transitional loosening of the compact structure would enable a rearrangement of the copper-site ligands. The difference in T_m between the 597 nm transitions, which monitors the structure of the copper site, and the DSC data for the oxidized samples (about 3−4 °C; see Table 1) could therefore reflect such a transition. In a similar manner, differences in the T_m of the unfolding transitions have been observed previously during thermal denaturation of oxidized spinach PC under aerobic conditions when monitored by absorbance spectroscopy (at 597 nm) or by DSC (*22*). The difference in T_ms was, however, reported to be significantly higher in this study: 7 °C at identical scan rates (60 °C h^{-1}) (*22*). Similar observations have been made for other cupredoxins (*40*−*42*). This thermally induced structural rearrangement of the copper site of cupredoxins has also been probed by EPR spectroscopy (*22*, *25*, *40*−*42*). In the majority of cases, however, the EPR signal is consistent with unspecific binding of the Cu^{2+} ion to backbone N- or O-atoms after protein denaturation and need therefore not reflect intermediates. Only in the case of anaerobic thermal denaturation of oxidized azurin has a proper intermediate been identified, having unusual EPR parameters ($A_{||} = 209$ and $g_{||} = 2.134$) indicative of a type 2 copper site with at least one cysteine ligand (*25*).

The thermal unfolding of reduced PC in the presence of dissolved molecular oxygen was, in contrast with the anaerobic sample, a remarkably more complex process (Figure 4). The first calorimetric endotherm was estimated to have a T_m of 71 °C, in analogy with the reversible anaerobic transition (see Table 1). Multiple exothermic processes abruptly disrupted this transition. An exothermic maximum was observed at approximately 80 °C, after which it decreased and leveled off at 85 °C. The exothermic phase returned to the baseline at about 95 °C. It should be noted that the small endothermic peak at 77 °C was fully reproducible (data not shown), but the significance of this finding is not understood. In analogy with the foregoing, aerobic thermal denaturation of oxidized PC is equally complex (Figure 5). Notable differences include the absence of the small peak at 77 °C and the occurrence of two exothermic dips. Alternatively, the exothermic dip in this (or both) aerobic sample(s) may be interrupted by an endothermic reaction.

The DSC result for the anaerobic oxidized sample (Figure 6A,B) is also nontrivial, with apparent multiple endotherms. For reasons discussed below, we believe that during the thermal melting of this sample there is formation of disulfide dimers. Since these dimers appear to have a higher T_m, an exothermic refolding of these would distort the profile unless dimerization occurs between folded proteins. Upon examination of the calorimetric profile in Figure 6A, the latter appears to be the case and is consistent with a pre-transitional disruption of the copper site thereby enabling such an intermolecular reaction.

Comparing the aerobic DSC transitions (Figures 4 and 5) with the DSC (Figure 6A,B), absorbance (Figure 6C), ESI MS (not shown), and size-exclusion linked DLS (Figure 7) data for the anaerobic oxidized sample, it is apparent that copper-site disulfide-linked dimers are formed and that these exhibit full reversibility and melt at a higher temperature than the monomeric wild type. Indeed, the copper site in PC is close to the surface (Figure 1), and soluble disulfide-linked dimers are readily obtained during anaerobic denaturation of oxidized PC using guanidinium (A. Sandberg, unpublished results). Furthermore, the accessible copper-site could easily accommodate an oxidized sulfur moiety in analogy with recent findings on the thermal denaturation of the azurin His117Gly mutant (*43*). This implies that the two small peaks seen upon a rescan of aerobically denatured PC correspond to monomeric protein (at 53 °C) and disulfide-bonded dimers (at 75−79 °C), which are further corroborated by the ESI MS species 10413 Da (nonoxidized monomer), 10449 Da (oxidized monomer; RSO_2H has a molecular weight of 10445 Da), and 20824 Da (dimeric species). The observation of two populations in size-exclusion linked DLS (Figure 7) is consistent with this interpretation. However, we are unable to explain the origin of the two minor species detected with masses of 20923 and 21023 Da.

It is evident from Figures 4 and 5 that dissolved oxygen is responsible for the exothermic oxidation reactions occurring at $T > T_m$ and that this causes irreversibility. Comparing the DLS and ESI MS data presented here with the aerobic thermal denaturation of reduced and oxidized azurin (*25*), it is clear that the copper ion catalyzes cysteine oxidation to sulfinic acid (RSO_2H) and disulfide ($RSS'R'$). It is increasingly becoming understood that not only oxygen but also sulfur and selenium of the chalcogens are important oxidative stressors in biological systems (*44*). Because of the electronic configuration of sulfur ($[Ne]3s^23p^4$), this atom is frequently involved in atom-exchange reactions and can have a wide array of oxidation states (up to +6) (*44*). As thiolate (RS^-), the oxidation state is −2 for the sulfur atom. However, the oxidation-states of −1 (as seen for the disulfide sulfurs), +4 (as seen in sulfinic acid), and +6 (as observed in sulfonic acid; RSO_3H) appear to be the only stable forms of oxidized sulfur species under physiological conditions. A previous report of oxidation of the metal-coordinating cysteine in apoazurin to sulfonic acid (*43*) reflects this tendency, which is merely the result of the different mechanisms of oxidation. When catalyzed by the copper ion, the short-lived thiyl radical ($RS^\bullet$; oxidation state of −1) and superoxide (O_2^-) appear to be intermediates resulting in a relatively stable sulfinic acid as opposed to direct attack by molecular oxygen, which would result in a species with the unstable oxidation state of +2 on the sulfur. We therefore believe that oxidation of the aerobic PC samples occurs via the following mechanisms:

$$RS^-{-}Cu^{2+} + O_2 \rightarrow [\, RS^\bullet + Cu^+ + O_2 \rightarrow RS^\bullet + Cu^{2+} + O_2^-\,] \rightarrow RSO_2^- + Cu^{2+} \quad (2)$$

$$RS^-{-}Cu^{+} + O_2 \rightarrow [\, RS^-{-}Cu^{2+} + O_2^- \rightarrow RS^\bullet + Cu^+ + O_2^-\,] \rightarrow RSO_2^- + Cu^{+} \quad (3)$$

The ability of the cuprous ion to reduce oxygen to superoxide has been demonstrated previously (*45*). Oxidation

of sulfinic acid into the fully oxidized sulfonic acid occurs during harsher conditions and prolonged denaturation times. It should be mentioned that recent attempts to spin-trap the thiyl radical in this reaction using oxidized wild-type azurin under anaerobic conditions by denaturation with both heat and guanidinium (the latter on ice) have failed (A. Sandberg and T. Vänngård, unpublished data), suggesting a fast reaction mechanism. This, in combination with the slowness of the DSC data, suggests that the reaction requires the simultaneous presence of all three reaction partners to proceed to product. Thus, autoxidation of the sulfur might not occur independently but via a transient complex involving two cysteines and at least one copper ion.

Of course, combination of two thiyl radicals into disulfide predominates in the absence of oxygen (but also occurs in the presence of oxygen):

$$R_1S_1^-{-}Cu^{2+} + R_2S_2^-{-}Cu^{2+} \rightarrow [\,R_1S_1^{\bullet} + R_2S_2^{\bullet} + 2Cu^{+}] \rightarrow R_1S_1S_2R_2 + 2Cu^{+} \quad (4)$$

On the basis of the above, we propose the following explanation for the complex DSC profiles: the exotherm results mostly from redox reactions 2 and 3 involving oxygen. Disulfide formation (reaction 4) occurs concomitantly with these reactions but is apparently not very exothermic, as can be seen in Figure 6A. Then, as the residual structure of the disulfide-linked monomers melt, there is a small endotherm around 75−79 °C. The exotherm returns to the baseline when all the oxygen is consumed. The occurrence of two transitions, monomeric and dimeric, is corroborated by the absorbance data presented in Figures 5C and 6C.

In previous studies, the aerobic heating of reduced spinach PC resulted in the formation of at least two final states, D1 and D2 (*21*). These forms were further characterized, and the D1 was described as an irreversibly denatured form having undergone an irreversible oxidation. The D2 form was suggested to be apo-PC based on its ability to refold under reducing conditions and with the addition of copper. However, a second possibility not noted in this study is that D2 may also represent disulfide dimers that too would refold under such conditions. Our DSC rescans of aerobic samples support the proposal that apo-PC is one of the final denatured states, as a small endothermic peak was observed with a T_m of approximately 53 °C, similar to the T_m of apo-Pc (T_m = 55 °C) (*46*). However, based on mass-spectrometric results presented here and previously (*25*, *43*), we are inclined to believe that our apo-PC is in fact oxidized to sulfinic acid, thus probably unable to bind metal.

Thus, it appears as if it is the complex redox chemistry of the cysteine sulfur that confers thermal irreversibility on the cupredoxin fold. However, reversible apparent two-state unfolding of PC and azurin is in stark contrast with previous claims of complex denaturation pathways involving one or several intermediates found for the cupredoxin amicyanin (*42*). Amicyanin shares 25 and 16% sequence identity with PC and azurin, respectively, yet their structures are similar as are most of the cupredoxins. On the basis of the results presented here and previously (*25*), we believe that this report (*42*) reflects the redox chemistry occurring in the denatured state instead of being accounts of proper intermediates. Furthermore, we speculate that the great majority of the cupredoxins will exhibit reversible thermal unfolding in an anaerobic environment but only as apo-protein, reduced (Cu^+), or reconstituted with a nonreducible metal ion (e.g., Zn^{2+}) instead of Cu^{2+}. Possibly, this will apply to other cysteine-ligating metal-binding proteins as well.

ACKNOWLEDGMENT

We are grateful to Stefan Geschwindner at the Structural Chemistry Laboratory, AstraZeneca Mölndal, Sweden, for the use of their VP-DSC calorimeter (Microcal). We would also like to thank Tore Vänngård for valuable comments. Hasse Karlsson at Medical Biochemistry, Göteborg University, Sweden, is acknowledged for the mass spectrometry measurements.

REFERENCES

1. Sykes, A. G. (1991) Plastocyanin and the blue copper proteins, *Struct. Bond. 75*, 175−224.
2. Sigfridsson, K. (1998) Plastocyanin, an electron-transfer protein, *Photosynth. Res. 57*, 1−28.
3. Gross, E. L. (1993) Plastocyanin: structure and function, *Photosynth. Res. 37*, 103−116.
4. Colman, P. M., Freeman, H. C., Guss, J. M., Murata, M., Norris, V. A., Ramshaw, J. A. M., and Venkatappa, M. P. (1978) The structure of plastocyanin determined by X-ray diffraction at 2.7 Å resolution, *Nature 272*, 319−324.
5. Xue, Y., Ökvist, M., Hansson, Ö., and Young, S. (1998) Crystal structure of spinach plastocyanin at 1.7 Å resolution, *Protein Sci. 7*, 2099−2105.
6. Bergkvist, A. Protein structure and interaction studied by NMR: Spinach plastocyanin and *Escherichia coli* transhydrogenase, Ph.D. Thesis, Göteborg University, Sweden, 2000.
7. Bertini, I., Bryant, D. A., Ciurli, S., Dikiy, A., Fernandez, C. O., Luchinat, C., Safarov, N., Vila, A. J., and Zhao, J. (2001) Backbone dynamics of plastocyanin in both oxidation states. Solution structure of the reduced form and comparison with the oxidized state, *J. Biol. Chem. 276*, 47217−47226.
8. Gray, H. B., Malmström, B. G., and Williams, R. J. (2000) Copper coordination in blue proteins, *J. Biol. Inorg. Chem. 5*, 551−559.
9. Ejdebäck, M., Bergkvist, A., Karlsson, B. G., and Ubbink, M. (2000) Side-chain interactions in the plastocyanin−cytochrome *f* complex, *Biochemistry 39*, 5022−5027.
10. Ubbink, M., Ejdeback, M., Karlsson, B. G., and Bendall, D. S. (1998) The structure of the complex of plastocyanin and cytochrome *f*, determined by paramagnetic NMR and restrained rigid-body molecular dynamics, *Structure 6*, 323−335.
11. Crowley, P. B., Otting, G., Schlarb-Ridley, B. G., Canters, G. W., and Ubbink, M. (2001) Hydrophobic interactions in a cyanobacterial plastocyanin−cytochrome *f* complex, *J. Am. Chem. Soc. 123*, 10444−10453.
12. Olesen, K., Ejdebäck, M., Crnogorac, M. M., Kostic, N. M., and Hansson, Ö. (1999) Electron transfer to photosystem 1 from spinach plastocyanin mutated in the small acidic patch: ionic strength dependence of kinetics and comparison of mechanistic models, *Biochemistry 38*, 16695−16705.
13. Schlarb-Ridley, B. G., Bendall, D. S., and Howe, C. J. (2002) Role of electrostatics in the interaction between cytochrome *f* and plastocyanin of the cyanobacterium *Phormidium laminosum*, *Biochemistry 41*, 3279−3285.
14. Schlarb-Ridley, B. G., Navarro, J. A., Spencer, M., Bendall, D. S., Hervas, M., Howe, C. J., and De La Rosa, M. A. (2002) Role of electrostatics in the interaction between plastocyanin and photosystem I of the cyanobacterium *Phormidium laminosum*, *Eur. J. Biochem. 269*, 5893−5902.
15. Makhatadze, G. I., and Privalov, P. L. (2000) Energetics of protein structure, *Adv. Protein Chem. 47*, 307−425.
16. Privalov, G. P., and Privalov, P. L. (2000) Problems and prospects in microcalorimetry of biological macromolecules, *Methods Enzymol. 323*, 31−62.
17. Privalov, P. L., and Potekhin, S. A. (1986) Scanning microcalorimetry in studying temperature-induced changes in proteins, *Methods Enzymol. 131*, 4−51.

18. Zale, S. E., and Klibanov, A. M. (1986) Why does ribonuclease irreversibly inactivate at high temperatures? *Biochemistry 25*, 5432−5444.
19. Volkin, D. B., and Klibanov, A. M. (1987) Thermal destruction processes in proteins involving cystine residues, *J. Biol. Chem. 262*, 2945−2950.
20. Tomazic, S. J., and Klibanov, A. M. (1988) Mechanisms of irreversible thermal inactivation of *Bacillus* α-amylases, *J. Biol. Chem. 263*, 3086−3091.
21. Gross, E. L., Draheim, J. E., Curtiss, A. S., Crombie, B., Scheffer, A., Pan, B., Chiang, C., and Lopez, A. (1992) Thermal denaturation of plastocyanin: the effect of oxidation state, reductants, and anaerobicity, *Arch. Biochem. Biophys. 298*, 413−419.
22. Milardi, D., La Rosa, C., Grasso, D., Guzzi, R., Sportelli, L., and Fini, C. (1998) Thermodynamics and kinetics of the thermal unfolding of plastocyanin, *Eur. Biophys. J. 27*, 273−282.
23. Sanchez-Ruiz, J. M. (1992) Theoretical-analysis of Lumry−Eyring models in differential scanning calorimetry, *Biophys. J. 61*, 921−935.
24. Milardi, D., La Rosa, C., and Grasso, D. (1994) Extended theoretical analysis of irreversible protein thermal unfolding, *Biophys. Chem. 52*, 183−189.
25. Sandberg, A., Leckner, J., Shi, Y., Schwarz, F. P., and Karlsson, B. G. (2002) Effects of metal ligation and oxygen on the reversibility of the thermal denaturation of *Pseudomonas aeruginosa* azurin, *Biochemistry 41*, 1060−1069.
26. Ejdebäck, M., Young, S., Samuelsson, A., and Karlsson, B. G. (1997) Effects of codon usage and vector-host combinations on the expression of spinach plastocyanin in *Escherichia coli*, *Protein Expr. Purif. 11*, 17−25.
27. Draheim, J. E., Anderson, G. P., Duane, J. W., and Gross, E. L. (1986) Plastocyanin conformation—an analysis of its near-ultraviolet absorption and circular dichroic spectra, *Biophys. J. 49*, 891−900.
28. Kirchhoff, W. H. (1993) Exam: a two-state thermodynamic analysis program, *NIST Tech. Note 1401*, 1−103.
29. Pace, C. N., and Scholtz, J. M. (1996) Measuring the conformational stability of a protein, in *Protein Structure: A Practical Approach* (Creighton, T. E., Ed.) pp 299−321, IRL Press, Oxford, UK.
30. Santoro, M. M., and Bolen, D. W. (1988) Unfolding free energy changes determined by the linear extrapolation method. 1. Unfolding of phenylmethanesulfonyl α-chymotrypsin using different denaturants, *Biochemistry 27*, 8063−8068.
31. Raiford, D. S., Fisk, C. L., and Becker, E. D. (1979) Calibration of methanol and ethylene glycol nuclear magnetic resonance thermometers, *Anal. Chem. 51*, 2050−2051.
32. Driscoll, P. C., Hill, H. A., and Redfield, C. (1987) ^{1}H NMR sequential assignments and cation-binding studies of spinach plastocyanin, *Eur. J. Biochem. 170*, 279−292.
33. Baker, D. (2000) A surprising simplicity to protein folding, *Nature 405*, 39−42.
34. Wedemeyer, W. J., Welker, E., Narayan, M., and Scheraga, H. A. (2000) Disulfide bonds and protein folding, *Biochemistry 39*, 4207−4216.
35. Pace, C. N., Grimsley, G. R., Thomson, J. A., and Barnett, B. J. (1988) Conformational stability and activity of ribonuclease T1 with zero, one, and two intact disulfide bonds, *J. Biol. Chem. 263*, 11820−11825.
36. Koide, S., Dyson, H. J., and Wright, P. E. (1993) Characterization of a folding intermediate of apoplastocyanin trapped by proline isomerization, *Biochemistry 32*, 12299−12310.
37. Seemann, H., Winter, R., and Royer, C. A. (2001) Volume, expansivity, and isothermal compressibility changes associated with temperature and pressure unfolding of *Staphylococcal* nuclease, *J. Mol. Biol. 307*, 1091−1102.
38. Ervin, J., Larios, E., Osvath, S., Schulten, K., and Gruebele, M. (2002) What causes hyperfluorescence: folding intermediates or conformationally flexible native states? *Biophys. J. 83*, 473−483.
39. Azuaga, A. I., Dobson, C. M., Mateo, P. L., and Conejero-Lara, F. (2002) Unfolding and aggregation during the thermal denaturation of streptokinase, *Eur. J. Biochem. 269*, 4121−4133.
40. La Rosa, C., Milardi, D., Grasso, D., Guzzi, R., and Sportelli, L. (1995) Thermodynamics of the thermal unfolding of azurin, *J. Phys. Chem. 99*, 14864−14870.
41. Guzzi, R., Sportelli, L., La Rosa, C., Milardi, D., Grasso, D., Verbeet, M. P., and Canters, G. W. (1999) A spectroscopic and calorimetric investigation on the thermal stability of the Cys3Ala/Cys26Ala azurin mutant, *Biophys. J. 77*, 1052−1063.
42. La Rosa, C., Milardi, D., Grasso, D. M., Verbeet, M. P., Canters, G. W., Sportelli, L., and Guzzi, R. (2002) A model for the thermal unfolding of amicyanin, *Eur. Biophys. J. 30*, 559−570.
43. Pozdnyakova, I., and Wittung-Stafshede, P. (2002) If space is provided, bulky modification on the rim of azurin's β-barrel results in folded protein, *FEBS Lett. 531*, 209−214.
44. Giles, G. I., and Jacob, C. (2002) Reactive sulfur species: an emerging concept in oxidative stress, *Biol. Chem. 383*, 375−388.
45. Günther, M. R., Hanna, P. M., Mason, R. P., and Cohen, M. S. (1995) Hydroxyl radical formation from cuprous ion and hydrogen peroxide: a spin-trapping study, *Arch. Biochem. Biophys. 316*, 515−522.
46. Datta, D., and Mayo, S. L. (2002) A designed apoplastocyanin variant that shows reversible folding, *Biochem. Biophys. Res. Commun. 296*, 988−990.
47. Guex, N., and Peitsch, M. C. (1997) SWISS-MODEL and the Swiss-PdbViewer: An environment for comparative protein modeling, *Electrophoresis 18*, 2714−2723.

BI034371E